

AAG: Self-Supervised Representation Learning by Auxiliary Augmentation with GNT-Xent Loss

Yanlun Tu¹, Jianxing Feng², Yang Yang^{1*}

¹ Department of Computer Science and Engineering,
Shanghai Jiao Tong University, Shanghai, China.

² Haohua Technology Co., Ltd, Shanghai, China.

tuyanlun@sjtu.edu.cn, fengjianxing@harmon.health, yangyang@cs.sjtu.edu.cn

Abstract

Self-supervised representation learning is an emerging research topic for its powerful capacity in learning with unlabeled data. As a mainstream self-supervised learning method, augmentation-based contrastive learning has achieved great success in various computer vision tasks that lack manual annotations. Despite current progress, the existing methods are often limited by extra cost on memory or storage, and their performance still has large room for improvement. Here we present a self-supervised representation learning method, namely AAG, which is featured by an auxiliary augmentation strategy and GNT-Xent loss. The auxiliary augmentation is able to promote the performance of contrastive learning by increasing the diversity of images. The proposed GNT-Xent loss enables a steady and fast training process and yields competitive accuracy. Experiment results demonstrate the superiority of AAG to previous state-of-the-art methods on CIFAR10, CIFAR100, and SVHN. Especially, AAG achieves 94.5% top-1 accuracy on CIFAR10 with batch size 64, which is 0.5% higher than the best result of SimCLR with batch size 1024.

Introduction

Image representation has always been the focus of computer vision studies. At the early developmental stage of image processing, images are represented by manually extracted global features (Jain and Vailaya 1996; Manjunath and Ma 1996), including color, texture, and edge information. As these features are sensitive to variable lighting conditions and occlusion, they have been largely replaced by local feature extractors, like BoW (Sivic and Zisserman 2003) and SIFT (Lowe 2004), while the representation ability has still been limited by the hand-crafted extracting rules.

For the past decade, automatic feature learning by deep neural networks (DNNs) has dominated the field of image representation. DNNs learn feature embeddings through multiple layers of non-linear transformations. The output high-level abstract features generalize well in various downstream tasks. Especially, convolutional neural networks trained on images with annotated class labels can capture visual similarity among different categories to successfully make a semantic classification. However, due to the high

cost or expertise required for manual annotation, a substantial ratio of image data remains unlabeled, which has not been effectively exploited.

In recent years, self-supervised learning methods (Jing and Tian 2019) have achieved breakthrough performance in the field of computer vision. The key to the success of these methods lies in the design of pretext tasks. As a special form of unsupervised learning, the “label” in self-supervised learning is derived from the data itself. Proper pretext tasks can make full use of the inherent properties of data to improve the quality of learned representation and enhance the performance of downstream tasks. Typical pretext tasks include image generation (Goodfellow et al. 2014), colorization (Zhang, Isola, and Efros 2016), inpainting (Pathak et al. 2016), and super resolution (Ledig et al. 2016), which focus on specific operation but can also have good generalization ability on downstream tasks. Another kind of pretext tasks is context-based methods (Doersch, Gupta, and Efros 2015; Noroozi and Favaro 2016; Gidaris, Singh, and Komodakis 2018), which utilizes spatial relations among different image patches or intrinsic attributes of images.

In this study, we focus on the task of instance-wise discrimination based on data augmentation, which is commonly-used in self-supervised learning. To create positive and negative labels, data augmentation techniques are utilized to generate views of images. The pairs of views originated from the same image form positive samples, and those from different images form negative samples. This kind of representative methods mainly includes batch-based and memory bank-based methods. A major limitation of these methods is the extra cost on storing the features of samples. For instance, the memory bank-based methods (Wu et al. 2018; Huang et al. 2019; Han et al. 2020) allocate large memory space to maintain the features of generated views for all samples. MoCo (He et al. 2019) also requires to build a queue for feature storage, while the differences lie on the encoder for generating features of keys and the variable length of the queue. Instead, SimCLR (Chen et al. 2020) directly fetches samples from batches. To ensure good performance, SimCLR has a much larger batch size, which restricts its applications in the labs of limited computational resources.

Therefore, how to get a comparable or even better result with less resource consumption has become an attrac-

tive topic in the self-supervised learning field. Considering that the end-to-end methods are more straightforward and flexible compared to memory bank and momentum-based methods, we mainly focus on the batch-based methods. To address the above challenge, we propose AAG, i.e. self-supervised representation learning by Auxiliary Augmentation with GNT-Xent Loss. Specifically, to obtain recognizable features, a self-supervised pretext task based on instance discrimination is adopted. The main idea is to treat each image instance as a single “class” so that the model has a direction for training.

The AAG model is driven by a hybrid data augmentation scheme using both basic and auxiliary data augmentation strategies, which generate three enhanced views for each image. Combinations of these views compose positive and negative samples that are fed into a siamese neural network to encode image features. Besides, to speed up the model training process while maintaining stability, we propose a simple but efficient contrastive loss function named GNT-Xent Loss. Optimizing this modified contrastive loss enforces the positive pairs more closer while negative pairs more separated, thus yielding more discriminative representations of images. This method not only gets rid of memory bank but also uses a much smaller batch size compared to previous batch-based methods.

To assess the discriminant ability of the learned representation, we use both weighted k NN algorithm and linear evaluation to evaluate the model performance. The contributions of our work are summarized as follows.

- We design a new scheme of contrastive learning with basic and auxiliary data augmentation. The hybrid data augmentation strategy greatly alleviates the dependency on large batch size.
- We propose a novel contrastive loss function which can not only maintain the stability of the training process but also improve the accuracy under both k NN and linear evaluation.
- The AAG method achieves SOTA accuracies on multiple benchmark datasets with low computation cost.

Related Work

In this section, we provide a brief overview of research progress on self-supervised representation learning in recent years, mainly involving contrastive learning.

Contrastive learning uses contrastive loss function to measure the distance between samples (Hadsell, Chopra, and Lecun 2006). The main idea is to first learn the low-dimensional mapping of raw data, then decrease the Euclidean distance of similar pairs and increase that of dissimilar pairs. It allows us to retain the original semantics of samples even when the dimensions are greatly reduced. Contrastive learning is an effective method to learn the common representation of samples in different categories.

Memory bank-based methods compute the contrastive loss by using the image representation stored in the memory bank with features of current minibatch (Wu et al. 2018;

Wu, Efron, and Yu 2018; He et al. 2019; Huang et al. 2019; Han et al. 2020). The memory bank itself will be updated iteratively during the training process. Wu et al. (2018) proposed a memory bank with appropriate parameter settings for the first time in the field of unsupervised learning. Then MoCo (He et al. 2019) replaces the memory bank with a variable length queue and achieves breakthrough results on a large-scale dataset.

Batch-based methods compute the contrastive loss in the current batch during the training process (Ye et al. 2019; Chen et al. 2020). The advantage of these methods is that the features for comparison are up-to-date at every time step. ISIF (Ye et al. 2019) shows the superiority of batch-wise contrastive learning. SimCLR (Chen et al. 2020) uses a quite large batch size to train the network with diversiform data augmentation approaches and achieves impressive results under the protocol of linear evaluation.

Methodology

Model Overview

To fully exploit the potential of self-supervised learning in extracting features from images, we propose Auxiliary Augment with GNT-Xent loss (AAG) method. The overview of our method is illustrated in Figure 1. Given a dataset of N images $\mathcal{D} = \{d_1, d_2, \dots, d_N\}$, our goal is to learn a function $v = f_\theta(d)$ without supervision, where $f_\theta(\cdot)$ is a deep neural network which maps image d to feature v . During the training process, we randomly sample a minibatch of n images at each iteration. For every image $d_i, i \in \{1, \dots, n\}$, we perform data augmentation for three times with basic augmentation and auxiliary augmentation. Three views are obtained by $core_{i,1} = g_{basic_1}(d_i)$, $core_{i,2} = g_{basic_2}(d_i)$ and $aux_i = g_{aux}(d_i)$, respectively, where g_{basic_1} and g_{basic_2} are sampled from the same family of basic augmentation while g_{aux} is sampled from auxiliary augmentation. Then we feed these three views into the backbone network and get three feature embeddings, $x_i = f_\theta(core_{i,1}), y_i = f_\theta(core_{i,2}), z_i = f_\theta(aux_i)$. Finally, we calculate GNT-Xent Loss as defined in Eq. (1). The loss is a sum of three components, each of which is the loss arising from differentiating a positive pair of views against the corresponding negative ones. The formal definitions of these three components are shown in Algorithm 1.

$$\mathcal{L}_i = \mathcal{L}_{x_i y_i} + \mathcal{L}_{z_i x_i} + \mathcal{L}_{z_i y_i} \quad (1)$$

For a comprehensive assessment on the quality of learned feature embeddings, we use two common evaluation methods, i.e. weighted k NN (Wu et al. 2018) and linear evaluation protocol (Bachman, Hjelm, and Buchwalter 2019; Chen et al. 2020).

Hybrid Data Augmentation Scheme

Data augmentation makes instance-wise discrimination a practical pretext task for self-supervised learning (SSL). As most of the downstream tasks depend on the discovery of high-level semantic meaning in images, a basic assumption of data augmentation-based SSL is that the semantic content

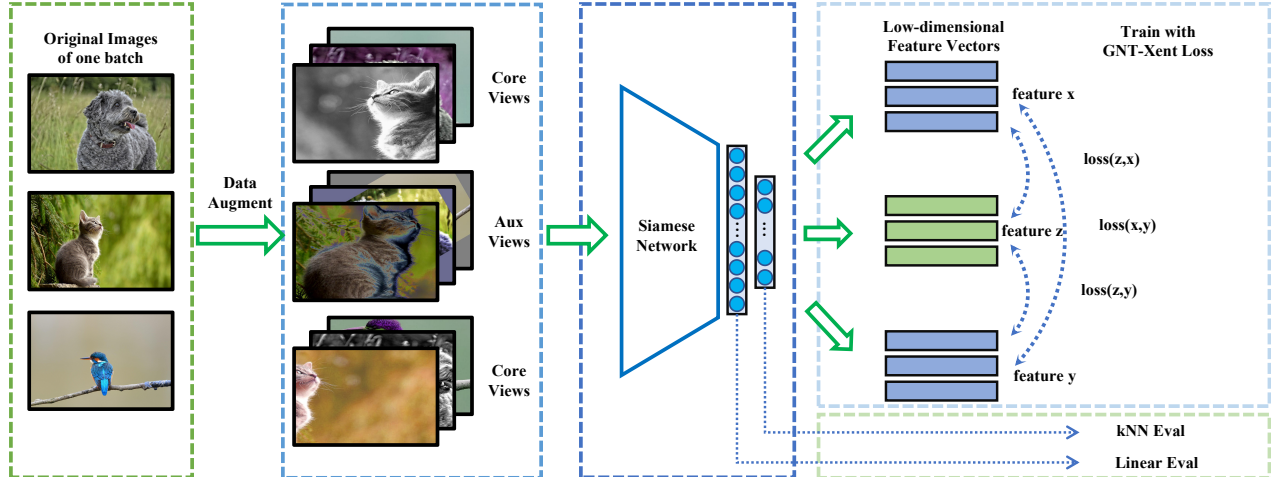


Figure 1: The framework of AAG. For one minibatch of each iteration in the training process, each image is enhanced with different data augmentation policies for three times, resulting into a triplet of views. These views are fed into a siamese network to extract low-dimensional feature vectors afterward. In the end, we calculate the GNT-Xent loss based on these features for optimization. We use both k NN and linear evaluation protocols to evaluate the learned representations.

of images is invariant to the augmentation operations. Thus, the basic goal of data augmentation is to bring diversification to image features and help the model distill the semantic information.

Basic data augmentation. Basic data augmentation is defined as the superposition of a series of random data augmentation approaches. Previous studies (Wu et al. 2018; Chen et al. 2020) have shown that data augmentation is crucial for image preprocessing. Whether data augmentation is applied properly determines the final result of the trained model. Following the practice of previous batch-based methods (Chen et al. 2020), our basic data augmentation consists of the following 5 operations that are performed sequentially with random magnitudes.

- i) Random resize and crop;
- ii) Color jitter;
- iii) Random grayscale;
- iv) Random horizontal flip;
- v) Gaussian blur.

By calling the basic data augmentation on an image twice, we obtain two views with different image attributes, which are called *core views*.

Auxiliary data augmentation. The basic data augmentation adopts a conservative scheme covering only five basic operations, which may be unable to generate sufficiently diversified image features. Some previous methods address this issue by increasing the number of samples, thus resulting into a large batch size. To reduce the dependency on batch size, we propose the auxiliary data augmentation strategy to generate additional views. The purpose of using auxiliary data augmentation is to bring in more data augmentation operations with more randomness so that the trained

model can learn the semantic information from images with various attributes.

Ideally, the more semantic-invariant transformations are included, the more easily models generalize well. However, the model performance does not necessarily benefit from adding augmentation operations, as the augmentation operations are not guaranteed to be semantic-invariant. The larger the operation pool, the higher risk may be introduced and further result into noisy samples in the dataset.

Therefore, to obtain a relatively reliable operation set, we choose good policies demonstrated by previous data augmentation studies, mainly from AutoAugment (Cubuk et al. 2019a) and RandAugment (Cubuk et al. 2019b). AutoAugment (Cubuk et al. 2019a) uses an adaptive search algorithm to find the best data augmentation policies for different datasets. The policy has several sub-policies. Each sub-policy consists of 2 operations which are associated with two values, i.e. the probability to use the operation and the magnitude of the operation. AutoAugment provides 25 best sub-policies for CIFAR10, SVHN, and ImageNet. The searched optimal policies can be used directly for the above datasets, while searching policies for a new dataset may be costly. RandAugment (Cubuk et al. 2019b) does not require a search process and only needs to define two parameters, namely the number of operations in a sub-policy and the magnitude of operations. It greatly reduces the time complexity of searching and achieves a close performance compared to AutoAugment.

Obviously, the operation pool for generating auxiliary views is much larger than that of basic augmentation. Therefore, to control the risk of introducing too much noise, we generate only one view for each image, which is called *auxiliary view*. In this way, there is no positive pair consisting

of two auxiliary views.

Pretext Task

Instance discrimination with three views. Instance discrimination (Wu et al. 2018) forces the model to learn to recognize different instances rather than different classes in the absence of any semantic labels. As a consequence, representations that capture the similarity and differences between instances can be learned. Although it is a task for discriminating instances, semantic insights can also be learned. Given three views for each image, the process of contrastive learning is as follows.

Suppose we have a minibatch of n images at some time step. The L2-normalized feature embeddings of the i th image are x_i , y_i , and z_i ($i \in \{1, \dots, n\}$), respectively, where x_i and y_i are derived from basic views, and z_i is derived from the auxiliary view. As we use cosine similarity to measure the distance between feature vectors, it is essential to apply L2norm to scale the length of vector to 1. Let $s(v_1, v_2) = v_1^\top v_2 / \|v_1\| \|v_2\|$ denote cosine similarity between two feature vectors v_1 and v_2 , then the value of $s(v_1, v_2)$ ranges from -1 to 1. In order to scale up the range of similarity, we follow (Wu et al. 2018) to apply a temperature parameter τ . With the above parameters, we propose a new loss function termed as GNT-Xent (the gradient-stabilized and normalized temperature-scaled cross-entropy loss), which is inspired by the name of NT-Xent (Chen et al. 2020). The GNT-Xent loss for a positive pair (x_i, y_i) is formulated as,

$$\mathcal{L}_{x_i y_i} = -\log \frac{\exp(s_i^+ / \tau)}{\sum_{k=1}^N \sum_{k \neq i} \exp(s_k^- / \tau)}, \quad (2)$$

where $s_i^+ = s(x_i, y_i)$ and $s_k^- = s(x_k, y_i)$ denote the similarity of a positive pair and negative pair, respectively (formal definitions are in Algorithm 1). The main definition from NT-Xent is that s^+ is removed from the denominator. Detailed explanations are given in the next section.

Design considerations of loss function. In this section, we will give a formal explanation on the reason for modifying NT-Xent. The original NT-Xent loss can be formulated as,

$$\mathcal{L}_{NT-Xent} = -\log \frac{\exp(s_i^+)}{\exp(s_i^+) + \sum_{k=1}^N \sum_{k \neq i} \exp(s_k^-)}, \quad (3)$$

where s_i^+ and s_k^- denote the similarity between a positive pair and a negative pair respectively. The loss above aims to minimize s_k^- and maximize s_i^+ . Thus the limit value of loss function approaches 0 on the right side. Actually, this limit is not required for contrastive learning, because contrastive learning only focuses on assimilating positive pairs while dissimilating negative pairs.

Based on this consideration, we propose a modified contrastive loss, GNT-Xent, as formulated in Eq. (4),

$$\mathcal{L}_{GNT-Xent} = -\log \frac{\exp(s_i^+)}{\sum_{k=1}^N \sum_{k \neq i} \exp(s_k^-)}, \quad (4)$$

As can be seen, the difference is that we subtract the item of the positive pair from the denominator. Let's

Algorithm 1 the overall learning algorithm of AAG.

Input: batch size n , dataset \mathcal{D} , temperature τ .

Output: network f_θ .

for each minibatch $\{d_i\}_{i=1}^n \in \mathcal{D}$ **do**

for all $i \in \{1, \dots, n\}$ **do**

 Draw augmentation functions

$g_{basic_1}, g_{basic_2} \sim \mathcal{G}_{basic}$ and $g_{aux} \sim \mathcal{G}_{aux}$

$x_i = f_\theta(g_{basic_1}(d_i))$

$y_i = f_\theta(g_{basic_2}(d_i))$

$z_i = f_\theta(g_{aux}(d_i))$

 Apply L2 norm to x_i, y_i, z_i

end for

for all $i \in \{1, \dots, n\}, j \in \{1, \dots, n\}, j \neq i$ **do**

$s_{x_i y_i}^+ = s(x_i, y_i) / \tau$

$s_{z_i x_i}^+ = s(z_i, x_i) / \tau$

$s_{z_i y_i}^+ = s(z_i, y_i) / \tau$

$s_{x_i x_j}^- = s(x_i, x_j) / \tau, s_{y_i y_j}^- = s(y_i, y_j) / \tau$

$s_{x_i y_j}^- = s(x_i, y_j) / \tau, s_{x_j y_i}^- = s(x_j, y_i) / \tau$

$s_{z_i x_j}^- = s(z_i, x_j) / \tau, s_{z_j x_i}^- = s(z_j, x_i) / \tau$

$s_{z_i y_j}^- = s(z_i, y_j) / \tau, s_{z_j y_i}^- = s(z_j, y_i) / \tau$

$\mathcal{L}_{x_i y_i} = -\log \frac{e^{s_{x_i y_i}^+}}{\sum_j e^{s_{x_i y_j}^-} + e^{s_{x_j y_i}^-} + e^{s_{x_i x_j}^-} + e^{s_{y_i y_j}^-}}$

$\mathcal{L}_{z_i x_i} = -\log \frac{e^{s_{z_i x_i}^+}}{\sum_j e^{s_{z_i x_j}^-}} \cdot \frac{e^{s_{z_i x_i}^+}}{\sum_j e^{s_{z_j x_i}^-}}$

$\mathcal{L}_{z_i y_i} = -\log \frac{e^{s_{z_i y_i}^+}}{\sum_j e^{s_{z_i y_j}^-}} \cdot \frac{e^{s_{z_i y_i}^+}}{\sum_j e^{s_{z_j y_i}^-}}$

end for

$\mathcal{L} = \frac{1}{n} \sum_{i=1}^n (\mathcal{L}_{x_i y_i} + \mathcal{L}_{z_i x_i} + \mathcal{L}_{z_i y_i})$

 Update siamese network f_θ to minimize \mathcal{L}

end for

Return the network f_θ

ignore the constant parameter τ and compute the gradients. $\frac{\partial \mathcal{L}_{NT-Xent}}{\partial s_i^+} = -\frac{\sum_{k=1}^N \sum_{k \neq i} \exp(s_k^-)}{\exp(s_i^+) + \sum_{k=1}^N \sum_{k \neq i} \exp(s_k^-)}$ and

$\frac{\partial \mathcal{L}_{NT-Xent}}{\partial s_k^-} = \frac{\exp(s_k^-)}{\exp(s_i^+) + \sum_{k=1}^N \sum_{k \neq i} \exp(s_k^-)}$. During the train-

ing, the value of s_i^+ keeps increasing rapidly, so gradients of $\frac{\partial \mathcal{L}_{NT-Xent}}{\partial s_i^+}, \frac{\partial \mathcal{L}_{NT-Xent}}{\partial s_k^-}$ will be affected and reduced. As a result, the training process can be hampered in the later stages. By contrast, the gradients of GNT-Xent will not be affected by the values of s_i^+ or s_k^- , because they are constant. It is trivial to deduce that $\frac{\partial \mathcal{L}_{GNT-Xent}}{\partial s_i^+} = -1$ and

$\frac{\partial \mathcal{L}_{GNT-Xent}}{\partial s_k^-} = \frac{\exp(s_k^-)}{\sum_{k=1, k \neq i}^N \exp(s_k^-)}$. The sum of $\frac{\partial \mathcal{L}_{GNT-Xent}}{\partial s_k^-}$

is 1. Then the training process can be steady and continuous.

The total loss of AAG consists of three components. As three positive pairs can be derived from three views for each image, each component aims to penalize for the prediction error of a positive pair. Here we have different treatments regarding the negative samples when calculating the losses. The major difference is that in the first component, we con-

sider all the core-core pairs of views from different images; while in the second and third components, although the positive pairs contain an auxiliary view, we do not take auxiliary-auxiliary pairs of views from different images into consideration. The major reason is that the auxiliary augmentation has much randomness and has more chances to produce noisy samples compared to basic augmentation.

Experiments

Experimental settings. To assess the performance of AAG working with different models, we experiment with three backbone networks, namely AlexNet (Krizhevsky, Sutskever, and Hinton 2012), ResNet18, and ResNet50 (He et al. 2016). For training the model, we set the batch size to 128 and the number of epochs to 200, and use SGD with momentum. The weight decay parameter is 5×10^{-4} and momentum is set to 0.9. The embedding feature size of the last layer is 128. The initial learning rate is 0.03. We replace the StepLR schedule with a CosineLR schedule (Loshchilov and Hutter 2016) without restarts. In the GNT-Xent loss, we set the temperature parameter τ to 0.1 as suggested in (Wu et al. 2018). In the experiments except the ablation study, we adopt the policies provided by AutoAugment as the default auxiliary augmentation policies. Most of the experiments were implemented in pytorch running on GeForce RTX 2080 Ti. And the experiments with large batch size were performed in Ascend 910 processor on Huawei Cloud.

Evaluation protocols. We adopt two common methods to evaluate the performance of self-supervised learning, namely k NN evaluation (Cover and Hart 1967; Wu et al. 2018) and linear evaluation (Zhang, Isola, and Efros 2016; Bachman, Hjelm, and Buchwalter 2019; Chen et al. 2020). The k NN evaluation computes low-dim features of the last layer and compares them against the ones of training images in the memory bank, using cosine similarity. The top k nearest neighbors will be used to make the prediction. Linear evaluation fixes parameters of the trained network and utilizes the features before the last layer to retrain a one-layer network. The accuracy of the one-layer network is regarded as the result of linear evaluation. We use Adam optimizer with the initial learning rate of 0.01 to train the one-layer network for 50 epochs. The CosineLR schedule is also applied.

Datasets. **CIFAR10** (Krizhevsky 2012) is a natural image dataset which contains 60000 color images of size 32×32 and 10 classes, among which 50000 images are for training and 10000 for testing. The image size of **CIFAR100** (Krizhevsky 2012) is the same as in CIFAR10, while CIFAR100 has 100 classes and each class has 600 images. In the **SVHN** dataset (Netzer et al. 2011), images were cropped patches of house numbers from the Google Street View images, which has 73257 images for training and 26032 for testing. The number of classes is 10 and the size of images is also 32×32 .

Results and Discussions

Baselines. We adopt six baseline models for comparison, including DeepCluster (Caron et al. 2018), Instance (Wu

et al. 2018), ISIF (Ye et al. 2019), AND (Huang et al. 2019), Super-AND (Han et al. 2020), and SimCLR (Chen et al. 2020).

Evaluation for short-term training. Table 1 describes the k NN evaluation on six models including the proposed AAG while excluding Super-AND, because Super-AND was trained for 5 rounds with 200 epochs per round (i.e. a total of 1000 epochs which is five times ours). For a fair comparison with Super-AND, we conduct another experiment shown in Table 2. From Table 1, we can see that without the memory bank, AAG still outperforms all baselines except for one case. And we find that by using a complex CNN, the performance of AAG can get more benefits. As a result, without using a memory bank, our method outperforms the state-of-the-art methods under the same condition with lower computation complexity.

Evaluation for long-term training. Experimental results show that AAG is far from convergence under the condition of 200 epochs. Table 3 shows that Super-AND performs a little bit better in the early stage but AAG achieves higher accuracy by a large margin in the later stage. It suggests that the accuracy of AAG can be further improved by more training epochs. Thus, we retrain our AAG for 1000 epochs on the above datasets. The results are shown in Table 2. AAG performs well with a longer training time under both k NN and linear evaluation.

Moreover, we experiment with different numbers of training epochs to investigate the impact of epoch number on the accuracy of k NN and linear evaluation on CIFAR10. As Figure 2 shows, the accuracy is improved as the number of epochs increases, and the accuracy of linear evaluation is always higher than that of k NN evaluation.

Investigation on batch size. To examine the effect of batch size in AAG, we conduct an experiment on CIFAR10 with varying batch size (Figure 3). We use $BatchSize/128 \times 0.03$ as the initial learning rate for the training of different batch sizes (Goyal et al. 2017). The training epoch is set to 200. For batch sizes more than 256, we warm up the learning rate for 10 epochs. The curve shows that the optimal batch size is not the largest one. The possible reason is that when the batch size gets larger, the positive samples being misclassified as negative pairs in a batch increases. Consequently, the overall performance declines.

Training process. To verify our theoretical analysis on GNT-Xent, we conduct a comparison experiment between GNT-Xent and NT-Xent (results shown in Figure 4). We use the same settings for both loss functions. As the values of gradients are influenced by the batch size, what we care about is the trend of changes rather than the specific value.

As can be seen, ∇s^+ and ∇s^- of GNT-Xent are constants during the training, whereas the values of NT-Xent decline sharply at the beginning and then going down steadily. As a result, the cosine similarity s^+ of GNT-Xent is higher than that of NT-Xent and the gap always exists. Furthermore, GNT-Xent achieves higher accuracy compared to NT-Xent. The results are reported in Table 4. Besides, to prove that

Table 1: k NN evaluation on different methods and datasets. Results marked as * are borrowed from previous work (Ye et al. 2019; Huang et al. 2019; Han et al. 2020)

Dataset (Network)	CIFAR10		CIFAR100		SVHN		Memory Bank
	ResNet18	AlexNet	ResNet18	AlexNet	ResNet18	AlexNet	
DeepCluster*	67.6	62.3	-	22.7	-	84.9	-
Instance*	80.8	60.3	50.7	32.7	93.6	79.8	✓
ISIF*	83.6	74.4	54.4	44.1	91.3	89.8	×
SimCLR*	82.3	73.0	55.8	43.2	90.8	88.6	×
AND*	86.3	74.8	57.2	41.5	94.4	90.9	✓
AAG (Ours)	88.3	74.9	60.6	39.7	95.3	92.6	×

Table 2: The results of AAG using both k NN and linear evaluation and Super-AND using k NN evaluation with 1000 training epochs.

Dataset (Network)	CIFAR10		CIFAR100		SVHN	
	ResNet18	AlexNet	ResNet18	AlexNet	ResNet18	AlexNet
Super-AND (k NN Eval)	89.2	75.6	61.5	42.7	94.9	91.9
AAG (k NN Eval)	91.2	81.2	64.9	50.0	95.6	93.0
AAG (Linear Eval)	91.6	81.2	66.4	51.2	96.3	94.3

Table 3: Comparison between Super-AND and AAG on CIFAR10 in a single training process of 1000 epochs under k NN evaluation.

Training epochs	200	400	600	800	1000
Super-AND	84.8	87.4	88.2	89.1	89.2
AAG	84.8	86.9	89.4	90.3	91.2

Table 4: Comparison between NT-Xent and GNT-Xent on CIFAR10 under k NN evaluation.

Loss	$lr = 0.03$	$lr = 0.3$
NT-Xent	86.8	84.2
GNT-Xent	88.3	86.1

Table 5: Comparison between NT-Xent and GNT-Xent on CIFAR10 with ISIF and SimCLR respectively.

Method	Evaluation	NT-Xent	GNT-Xent
ISIF	k NN	83.3	85.5
SimCLR	Linear	82.9	85.8

Table 6: Comparison with SimCLR and AMDIM on CIFAR10.

Method	Network	Batch Size	Linear Eval
AMDIM	ResNet50 (25 \times)	-	91.2
SimCLR	ResNet50 (MLP)	1024	94.0
AAG	ResNet50 (MLP)	64	94.5

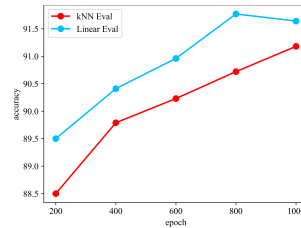


Figure 2: Impact of training epoch on CIFAR10.

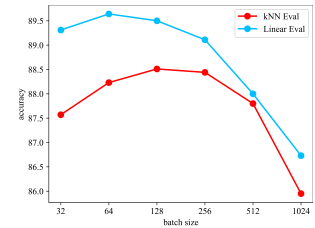


Figure 3: Impact of batch size on CIFAR10.

GNT-Xent does not simply speed up the learning process, we use a larger learning rate of 0.3 to retrain the model. Even though the performance of both loss functions gets worse, GNT-Xent still performs better than NT-Xent.

To further examine the efficacy of the proposed loss function, we conduct another comparison experiment with two existing methods (Ye et al. 2019; Chen et al. 2020) which use NT-Xent as their loss function. As shown in Table 5, we replace their loss functions by GNT-Xent. The modified versions outperform original ones by a large margin.

In addition, to visualize the discriminant capacity of learned features, we project the 128D features onto 2D space via the t-SNE algorithm (Maaten and Hinton 2008). As Figure 6 shows, the features of GNT-Xent has a more separated distribution than that of NT-Xent. The results shown in Figure 5, i.e. the curves of k NN accuracy and loss during the training, again demonstrate the advantages of GNT-Xent over NT-Xent.

Train with a bigger network. The SOTA method AMDIM (Bachman, Hjelm, and Buchwalter 2019) achieves an accuracy of 91.2% on CIFAR10 with ResNet50 (25 \times), while SimCLR outperforms AMDIM by using a larger batch

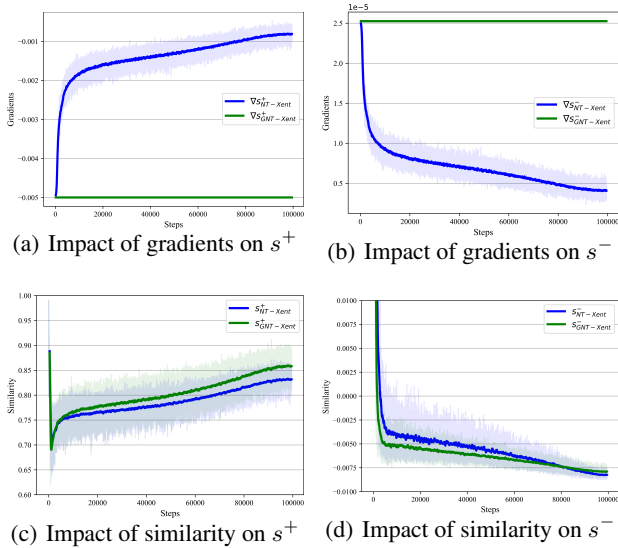


Figure 4: Comparison between NT-Xent and GNT-Xent on the values of ∇s^+ , ∇s^- , s^+ , and s^- at each iteration (Curve smoothing is applied).

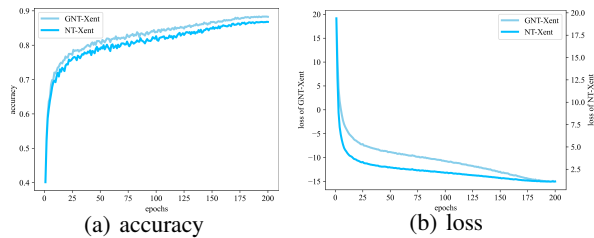


Figure 5: Curves of k NN accuracy and loss on CIFAR10 with different loss functions.

size and longer training steps with a standard ResNet50. To compare with SimCLR, we use the same network with a 2-layer MLP as SimCLR does and train for 1000 epochs. Note that different from SimCLR, we use a batch size of 64 which allows training on a single GPU like RTX 2080Ti. Table 6 shows that our method outperforms SimCLR’s best result with batch size 1024. This result suggests that the batch size can be effectively reduced by using our method.

Ablation study. To verify the validity of our method and investigate the impact of different components, we perform an ablation study with the following variants of AAG,

- i) Using only two basic views;
- ii) Replacing the auxiliary view with a basic view;
- iii) Replacing CosineLR schedule with StepLR schedule;
- iv) Replacing GNT-Xent loss with NT-Xent loss;
- v) Using RandAugment (2 random operations with a magnitude of 10) as the auxiliary augmentation approach.

Table 7 displays the k NN evaluation results on CIFAR10 and reveals that each component of AAG has a positive effect on improving the model accuracy. Among these vari-

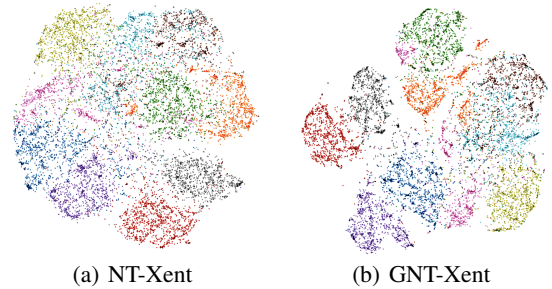


Figure 6: Visualization of features obtained by NT-Xent and GNT-Xent on CIFAR10.

ants, auxiliary data augmentation contributes most to the performance gain. It can be also observed that using policies of RandAugment achieves a close performance compared with that of using AutoAugment, indicating that the AAG method is relatively robust to the augmentation policies used to generate the auxiliary view. Thus, it is applicable to various datasets where the optimal policies are unavailable.

Table 7: Ablation study on CIFAR10.

Network	Accuracy
Full Model	88.3
Two Basic Views	85.8
Three Basic Views	86.9
with StepLR	87.1
with NT-Xent Loss	86.8
with RandAugment	88.1

Conclusion

In this paper, we focus on the augmentation-based self-supervised learning and develop a new method called AAG, which contains a new auxiliary augmentation scheme and a new GNT-Xent loss. The former introduces an auxiliary view in addition to the basic views to enhance the diversity of views and increase the number of data samples within a batch in the meantime. And the latter aims to achieve stable and efficient training. Both of these two components show advantages over their counterpart methods in the experiments. AAG improves the overall performance and works well in the condition of a small batch size which reduces space consumption, showing its great potential for unsupervised learning in computer vision tasks.

References

- Bachman, P.; Hjelm, R. D.; and Buchwalter, W. 2019. Learning representations by maximizing mutual information across views. In *Advances in Neural Information Processing Systems*, 15535–15545.
- Caron, M.; Bojanowski, P.; Joulin, A.; and Douze, M. 2018. Deep Clustering for Unsupervised Learning of Visual Features 139–156.

- Chen, T.; Kornblith, S.; Norouzi, M.; and Hinton, G. E. 2020. A Simple Framework for Contrastive Learning of Visual Representations. *arXiv: Learning* .
- Cover, T.; and Hart, P. 1967. Nearest neighbor pattern classification. *IEEE transactions on information theory* 13(1): 21–27.
- Cubuk, E. D.; Zoph, B.; Mane, D.; Vasudevan, V. K.; and Le, Q. V. 2019a. AutoAugment: Learning Augmentation Strategies From Data 113–123.
- Cubuk, E. D.; Zoph, B.; Shlens, J.; and Le, Q. V. 2019b. RandAugment: Practical automated data augmentation with a reduced search space. *arXiv: Computer Vision and Pattern Recognition* .
- Doersch, C.; Gupta, A.; and Efros, A. A. 2015. Unsupervised Visual Representation Learning by Context Prediction 1422–1430.
- Gidaris, S.; Singh, P.; and Komodakis, N. 2018. Unsupervised Representation Learning by Predicting Image Rotations .
- Goodfellow, I.; Pougetabadie, J.; Mirza, M.; Xu, B.; Wardefarley, D.; Ozair, S.; Courville, A.; and Bengio, Y. 2014. Generative Adversarial Nets 2672–2680.
- Goyal, P.; Dollár, P.; Girshick, R.; Noordhuis, P.; Wesolowski, L.; Kyrola, A.; Tulloch, A.; Jia, Y.; and He, K. 2017. Accurate, large minibatch sgd: Training imagenet in 1 hour. *arXiv preprint arXiv:1706.02677* .
- Hadsell, R.; Chopra, S.; and Lecun, Y. 2006. Dimensionality Reduction by Learning an Invariant Mapping 2: 1735–1742.
- Han, S.; Xu, Y.; Park, S.; Cha, M.; and Li, C. 2020. A Comprehensive Approach to Unsupervised Embedding Learning based on AND Algorithm. *arXiv: Learning* .
- He, K.; Fan, H.; Wu, Y.; Xie, S.; and Girshick, R. 2019. Momentum Contrast for Unsupervised Visual Representation Learning. *arXiv: Computer Vision and Pattern Recognition* .
- He, K.; Zhang, X.; Ren, S.; and Sun, J. 2016. Deep Residual Learning for Image Recognition 770–778.
- Huang, J.; Dong, Q.; Gong, S.; and Zhu, X. 2019. Unsupervised Deep Learning by Neighbourhood Discovery 2849–2858.
- Jain, A. K.; and Vailaya, A. 1996. IMAGE RETRIEVAL USING COLOR AND SHAPE. *Pattern Recognition* 29(8): 1233–1244.
- Jing, L.; and Tian, Y. 2019. Self-supervised Visual Feature Learning with Deep Neural Networks: A Survey. *arXiv: Computer Vision and Pattern Recognition* .
- Krizhevsky, A. 2012. Learning Multiple Layers of Features from Tiny Images. *University of Toronto* .
- Krizhevsky, A.; Sutskever, I.; and Hinton, G. E. 2012. ImageNet Classification with Deep Convolutional Neural Networks 1097–1105.
- Ledig, C.; Theis, L.; Huszar, F.; Caballero, J.; Cunningham, A.; Acosta, A.; Aitken, A. P.; Tejani, A.; Totz, J.; Wang, Z.; et al. 2016. Photo-Realistic Single Image Super-Resolution Using a Generative Adversarial Network. *arXiv: Computer Vision and Pattern Recognition* .
- Loshchilov, I.; and Hutter, F. 2016. Sgdr: Stochastic gradient descent with warm restarts. *arXiv preprint arXiv:1608.03983* .
- Lowe, D. G. 2004. Distinctive Image Features from Scale-Invariant Keypoints. *International Journal of Computer Vision* 60(2): 91–110.
- Maaten, L. v. d.; and Hinton, G. 2008. Visualizing data using t-SNE. *Journal of machine learning research* 9(Nov): 2579–2605.
- Manjunath, B. S.; and Ma, W. 1996. Texture features for browsing and retrieval of image data. *IEEE Transactions on Pattern Analysis and Machine Intelligence* 18(8): 837–842.
- Netzer, Y.; Wang, T.; Coates, A.; Bissacco, A.; Wu, B.; and Ng, A. Y. 2011. The Street View House Numbers (SVHN) Dataset .
- Noroozi, M.; and Favaro, P. 2016. Unsupervised Learning of Visual Representations by Solving Jigsaw Puzzles 69–84.
- Pathak, D.; Krahenbuhl, P.; Donahue, J.; Darrell, T.; and Efros, A. A. 2016. Context Encoders: Feature Learning by Inpainting 2536–2544.
- Sivic; and Zisserman. 2003. Video Google: a text retrieval approach to object matching in videos 1470–1477.
- Wu, Z.; Efros, A. A.; and Yu, S. X. 2018. Improving generalization via scalable neighborhood component analysis. In *Proceedings of the European Conference on Computer Vision (ECCV)*, 685–701.
- Wu, Z.; Xiong, Y.; Yu, S. X.; and Lin, D. 2018. Unsupervised Feature Learning via Non-parametric Instance Discrimination 3733–3742.
- Ye, M.; Zhang, X.; Yuen, P. C.; and Chang, S. 2019. Unsupervised Embedding Learning via Invariant and Spreading Instance Feature 6210–6219.
- Zhang, R.; Isola, P.; and Efros, A. A. 2016. Colorful Image Colorization 649–666.